Broglia, R. and Choi, K.-S. and Houston, Paul and Pasquale, L. and Zanchetta, Pericle (2018) Output feedback control of flow separation over an aerofoil using plasma actuators. International Journal of Numerical Analysis and Modeling . ISSN 1705-5105 (In Press)

INTERNATIONAL JOURNAL OF
NUMERICAL ANALYSIS AND MODELING
Volume 00, Number 0, Pages 000–000

OUTPUT FEEDBACK CONTROL OF FLOW SEPARATION OVER AN AEROFOIL USING PLASMA ACTUATORS

R. BROGLIA, K.-S. CHOI, P. HOUSTON, L. PASQUALE, AND P. ZANCHETTA

Abstract. We address the problem of controlling the unsteady flow separation over an aerofoil, using plasma actuators. Despite the complexity of the dynamics of interest, we show how the problem of controlling flow separation can be formulated as a simple set-point tracking problem, so that a simple control strategy may be used. A robust output feedback control is designed, on the basis of a low-order, linear, dynamical model approximating the incompressible Navier-Stokes equations, obtained from the snapshots of 2D laminar finite element simulations at $Re = 1,000$. Fast flow reattachment is achieved, along with both stabilisation and increase/reduction of the lift/drag, respectively. Accurate 2D finite element simulations of the full-order nonlinear equations illustrate the effectiveness of the proposed approach: good dynamic performances are obtained, as both the Reynolds number and the angle of attack are varied. The chosen output can be experimentally measured by appropriate sensors and, despite its simplicity, the proposed set-point tracking controller is sufficient to suppress the laminar separation bubble; moreover, its extension to 3D turbulent configurations is straightforward ([33, 7]), thus illustrating the effectiveness of the designed control algorithm in more practical conditions, which are far from the design envelope.

Key words. Feedback flow control, Robust control, Reduced-order modelling, Plasma actuators, Nonlinear systems.

1. Introduction

Closed-loop flow control is aimed at altering a natural flow state into a more desirable state, which is chosen depending on control objectives. Crucial examples are: manipulation of flow separation and flow reattachment, drag reduction, noise suppression, stall prevention, increasing mixing and combustion efficiency. Within this context, feedback controllers are pivotal, as they can achieve a full and efficient regulation of the flow field in real-time, see [18]. In particular, the incorporation of control theory into many open problems in fluid mechanics presents a host of new opportunities, with a wide range of applications in disparate fields (*e.g.* gas turbines, aircraft, as well as ground and marine vehicles).

The control input is usually an electric signal, which has to be converted to a physical quantity by means of an actuator. A new and original technology using non-thermal surface plasmas has witnessed a significant growth in interest in recent years, see [10, 12, 15, 31, 39], as they: have no moving parts; exhibit an extremely fast time-response; are characterised by low mass and low input power [8]. These surface dielectric barrier discharge (DBD) actuators are used to accelerate the near-wall flow, thus modifying the velocity profile within the boundary layer. The ionised fluid results in a localised body force vector field, which acts on the overlying neutrally charged fluid. The plasma actuator AC voltage can be used as a control input so that the generated force directly affects the flow over the aerofoil. However, the coupled neutrally-charged fluid and plasma dynamics are not trivial to model: neither the analytical model, which results in a system of nonlinear Partial Differential Equations (PDEs), nor the high-dimensional discretised dynamics, are suitable for control design purposes. Furthermore, the dependence of the dynamical

properties on both the unknown flow and geometry parameters is highly nonlinear. Therefore, it is very difficult to obtain an accurate control-oriented model. On the other hand, we show that the problem of controlling flow separation along the aerofoil can be formulated as a simple set-point tracking problem, so that a simple control strategy may be used. In particular, we aim to design a robust integral controller, on the basis of the recent results in [25], which however requires some stability conditions to be satisfied by the model. Then, the objective becomes to find a suitably accurate but "cheap" model, which allows for the design of such a simple controller.

In this regard, the introduction of a dedicated, reduced-order model (ROM), which is based on the explicit description of the flow dynamics, can convey a clearer understanding of the underlying physics of the problem, compared to system identification methods, see [9, 11]. One way of obtaining tractable ROMs is to project large-scale problems onto lower-dimensional subspaces, thus providing insight into the key spatial modes of fluid/structure systems, contrarily to black-box identification techniques, see [2]. The most popular model reduction technique in the control community is the balanced truncation, a classic method developed in [30] for stable, linear systems, which was extended in [41] to unstable, linear systems.

An approximated balanced truncation method, called balanced Proper Orthogonal Decomposition (POD), was extended in [34] to linear fluid systems and is based on a variant of the method proposed in [20], which forms approximate empirical Gramians. Moreover, the balanced POD was extended in [1] to unstable linear systems, when the dimension of the unstable subsystem is relatively small. The balanced POD projects the system onto the subspace spanned by the most observable and controllable modes and was shown to outperform the standard POD introduced in [22] for closed-loop flow control applications, see [4, 16]. Several authors have focused on the feedback control of balanced POD models, based on the Navier-Stokes equations, linearised about a single steady trajectory, see, for instance, [1, 4]. These linearisation-based approaches allows for the application of well-established linear model reduction methods. However, an accurate approximation of the nonlinear behaviour can only be obtained in a small neighbourhood of the considered trajectory, whose choice heavily affects the control performance. Moreover, the resulting model is unstable, in contrast with the typical stability properties of fluid systems. The key idea is then to take advantage of the effectiveness of this linear model reduction method, while avoiding the restrictions related to linearisation approaches.

A variant of the Arnoldi algorithm called Dynamic Mode Decomposition (DMD) was proposed in [36] to approximate part of the spectrum of the Koopman operator, see [19]. The latter is an infinite-dimensional linear operator describing the evolution of observables on the phase space, which has been used to analyse uncontrolled, nonlinear dynamical systems, see [28, 27, 29], evolving on an attractor. The article [35] showed that the DMD modes approximate some of the Koopman modes, which can be interpreted as the eigenmodes of a finite-dimensional linear map that approximates the true, nonlinear one. This method does not rely on linearisation of the dynamics: indeed, it captures the full information of the nonlinear system. On the other hand, the order of the DMD linear model is high and depends on the number of linearly independent snapshots needed to describe the dynamics of interest. Furthermore, there are no well-defined selection criteria for selecting the

DMD modes to be retained in the ROM, see [4], thereby making the use of DMD as a model reduction method less straightforward.

Recent works on feedback flow separation control using plasma actuators focused on either model-free or system identification based controllers. For instance, [6] proposed a slope-seeking algorithm to obtain maximum time-averaged lift, which is measured by a three-component balance. In [10], the authors proposed a retrospective cost adaptive algorithm to minimize the variation of the aerodynamic lift. The Eigensystem Realisation Algorithm (ERA) - a system identification method introduced in [17] - was applied to the impulse responses of the aerodynamic lift, in order to obtain a linear model, upon which the controller was designed. In [23] it is demonstrated that ERA yields the same ROMs as balanced POD, in the case of stable, linear systems but the physical meaning of the state-variables is lost. Furthermore, the aerodynamic lift, which is the chosen output in both [6] and [9], cannot be measured in real-time in realistic flow control applications.

Our objective is to solve the problem of directly controlling the unsteady flow separation using real-time velocity measurements, which are available in realistic applications, see, for instance, [15]. We propose this flow separation problem as a practical application of the new theoretical results in [25]. In particular, the aim of this paper is to show how, despite the high complexity of the system, a very simple robust output regulator is sufficient to effectively suppress the flow separation along an aerofoil, using a single DBD plasma actuator. First, a novel control-oriented ROM of the flow/actuator dynamics, whose state variables have a clear and consistent physical meaning, is proposed. The method combines DMD, as an alternative to linearisation, and balanced POD, as a way to select the most observable and controllable DMD modes. The high-order DMD model is projected using the balanced POD modes, thus yielding a balanced, stable, linear ROM. Furthermore, on the basis of the so-obtained model, we extend the recent results in [25] to a wider class of control systems and propose their application to this specific problem, which is of practical interest. Accurate finite element simulations of the full-order nonlinear equations are performed in order to test the control effectiveness and validate the modelling assumptions: they illustrate the robust performance, with respect to both parameter variations (*i.e.*, geometry of the domain and Reynolds number) and model uncertainties, of the proposed control algorithm.

It has to be noted that, although the linear ROM is obtained from the snapshots of 2D laminar finite element simulations at $Re = 1,000$, the proposed controller has been proved to be suitable for a more practical application, *i.e.*, to the laminar/turbulent transition control over a 3D wing at higher Reynolds numbers, see [33, 7], which are far from the design envelope.

2. Problem Statement and Objectives

This paper addresses the practical problem of robustly controlling the unsteady flow separation over an aerofoil, using the plasma actuator voltage as the control input and realistically available real-time velocity measurements as the control output. In particular, we aim to formulate and solve the flow separation problem, *i.e.*, to make

$$\partial_{\boldsymbol{n}} u_{\boldsymbol{\tau}}(t,\boldsymbol{x})|_{\Gamma_N} = \big(\boldsymbol{\tau}(\boldsymbol{x}) \cdot \nabla \boldsymbol{u}(t,\boldsymbol{x}) \cdot \boldsymbol{n}(\boldsymbol{x})\big)|_{\Gamma_N} > 0, \tag{1}$$

as a simple output regulation problem, *i.e.*, to make the measured output

$$\mathrm{y}(t) = u_\tau(t, \boldsymbol{x}_s) > \epsilon > 0. \tag{2}$$

Here, $\boldsymbol{u}$ is the time-dependent flow velocity vector; $\boldsymbol{x}$ and $\boldsymbol{x}_s$ denote the spatial coordinates and the sensor location, respectively; Γ_N represents the aerofoil boundary; $\boldsymbol{n}$ and $\boldsymbol{\tau}$ are the normal and tangent unit vectors to Γ_N, respectively. Our objective is to design a simple robust output feedback control, along with a suitable reference signal y^* for y, in order to suppress the flow separation along the aerofoil, *i.e.*, to drive the regulation error $\tilde{\mathrm{y}} = \mathrm{y} - \mathrm{y}^*$ to zero. To this end, we extend the recent results in [25] to a wider class of control-systems, which are suitable for our specific scenario, and propose their application to the flow separation control problem.

We assume there exist suitable references ϵ for the output $\mathrm{y}(t)$, which guarantee that, given a certain range for both Re and β, the solution of the output regulation problem (2) implies the solution of the flow separation problem (1). This is formalised by the following assumption.

Assumption 1. *For any $\delta \geq 0$ there exist some references $\epsilon > 0$, a $T_\epsilon > 0$ and a $T_\delta \geq T_\epsilon$ such that, if $y(t) > \epsilon$ for all $t > T_\epsilon$, then $\partial_{\boldsymbol{n}} u_{\boldsymbol{\tau}}(t, \boldsymbol{x})|_{\Gamma_N} > -\delta$ for all $t > T_\delta$, $Re \in \mathcal{R}_{Re} = [Re_m, Re_M]$, $\beta \in \mathcal{R}_\beta = [\beta_m, \beta_M]$.*

The resulting regulating control is designed upon a single ROM approximation of the nonlinear flow dynamics, for given parameters. The proposed control-oriented ROM is obtained from the snapshots of a finite element approximation of the 2D incompressible Navier-Stokes equations, which govern the evolution of $\boldsymbol{u}$, in the presence of a body force distribution, which represents the action of the plasma actuators on the neutrally-charged flow dynamics.

3. Control-oriented ROM

We obtain in this section a linear reduced-order representation of any nonlinear high-order system of the form: $\mathrm{x} = \mathrm{x}(t) : \mathbb{R} \to \mathbb{R}^n$, $\dot{\mathrm{x}} = \mathrm{d}\mathrm{x}/\mathrm{d}t$, $E \in \mathbb{R}^{n \times n}$, $\mathcal{F}(\cdot) : \mathbb{R}^n \to \mathbb{R}^n$, $G \in \mathbb{R}^{n \times p}$, $\mathrm{v} = \mathrm{v}(t) : \mathbb{R} \to \mathbb{R}^p$, $\mathrm{y} = \mathrm{y}(t) : \mathbb{R} \to \mathbb{R}^q$, such that

$$\begin{cases} E\dot{\mathrm{x}} &= \mathcal{F}(\mathrm{x}) + G\mathrm{v}, \\ \mathrm{y} &= H\mathrm{x}, \end{cases} \tag{3}$$

under the assumption that the open-loop asymptotic trajectories of the full-order nonlinear dynamics (3) in the phase space evolve towards finite dimensional attractors. Since a time-stepping is required, in order to compute the n states of system (3), a discrete-time setting is used in this section, to derive the ROM.

3.1. Preliminaries: Balanced POD. Consider a stable, linear system $(\bar{F}, \bar{G}, \bar{H})$ with m states, p inputs and q outputs. Let $\bar{\mathrm{x}}_1(t), ..., \bar{\mathrm{x}}_p(t)$ be the the state responses to unit impulses $\mathrm{v} = [\mathrm{v}_1(t), ..., \mathrm{v}_p(t)] = [\delta(t), ..., \delta(t)]$ and $\bar{\mathrm{z}}_1(t), ..., \bar{\mathrm{z}}_q(t)$ be the impulse responses of the adjoint system $(\bar{F}^{\mathrm{T}}, \bar{H}^{\mathrm{T}}, \bar{G}^{\mathrm{T}})$, where $(\cdot)^{\mathrm{T}}$ denotes the transpose of $(\cdot)$. Suppose the controllability and observability Gramians can be factorised as $W_c = XX^{\mathrm{T}}$, $W_o = ZZ^{\mathrm{T}}$, where $X = [\bar{\mathrm{x}}_1(t_1)\sqrt{\delta_1}, ..., \bar{\mathrm{x}}_1(t_{\bar{m}})\sqrt{\delta_{\bar{m}}}, ..., \bar{\mathrm{x}}_p(t_1)\sqrt{\delta_1}, ..., \bar{\mathrm{x}}_p(t_{\bar{m}})\sqrt{\delta_{\bar{m}}}]$ and $Z = [\bar{\mathrm{z}}_1(t_1), ..., \bar{\mathrm{z}}_1(t_{\bar{m}}), ..., \bar{\mathrm{z}}_p(t_1), ..., \bar{\mathrm{z}}_p(t_{\bar{m}})]$ are the snapshots matrices used to compute the empirical Gramians and δ_i are quadrature coefficients.

The balancing modes are computed by performing the Singular Value Decomposition (SVD) of the matrix $Z^{\mathrm{T}}X$:

$$Z^{\mathrm{T}}X = \begin{pmatrix} U_1 & U_2 \end{pmatrix} \begin{pmatrix} \Sigma_1 & 0 \\ 0 & 0 \end{pmatrix} \begin{pmatrix} V_1 \\ V_2 \end{pmatrix}^{\mathrm{T}}, \tag{4}$$

where $\Sigma_1 = \mathrm{diag}(\sigma_1, ..., \sigma_{r_1}) \in \mathbb{R}^{r_1 \times r_1}$ is a diagonal matrix, whose eigenvalues are all the non-zero Hankel singular values $\sigma_1 > \sigma_2 ... > \sigma_{r_1} > 0$, r_1 is the rank of $Z^{\mathrm{T}}X$, $U_1 \in \mathbb{R}^{m \times r_1}$, $V_1 \in \mathbb{R}^{r_1 \times r_1}$ and $U_1^{\mathrm{T}}U_1 = V_1^{\mathrm{T}}V_1 = I_{r_1}$, where $I_{r_1} \in \mathbb{R}^{r_1 \times r_1}$ is the identity matrix. Define the matrices $\Phi_r \in \mathbb{R}^{m \times r}$, $\Psi_r \in \mathbb{R}^{m \times r}$ as

$$\Phi_r = XV_1\Sigma_1^{-1/2}, \quad \Psi_r = ZU_1\Sigma_1^{-1/2}, \tag{5}$$

where $r \leq r_1$ can be chosen in order to neglect the smallest Hankel singular values in Σ_1. The columns of $\Phi_r = [\varphi_1, ..., \varphi_r]$ form the first r columns of the balancing transformation, e.g. the balancing modes. The rows of $\Psi_r^{\mathrm{T}} = [\psi_1, ..., \psi_r]^{\mathrm{T}}$ form the first r rows of the balancing transformation, e.g. the adjoint modes.

3.2. Preliminaries: DMD. Let $\mathrm{x}^{(k)} = \mathrm{x}(t_k) = \mathrm{x}(k\Delta t)$ be the iterates of the state, sampled at regular time intervals $k\Delta t$, where Δt is a fixed time step, which could be, as in the following, the finite element simulation time step. The DMD algorithm, proposed by [36], approximates the flow field $\mathrm{x}^{(k)}$ as the sum of the first m approximated Koopman modes, called DMD modes $\boldsymbol{\nu}_j$, weighted by the powers λ_j^k of their corresponding eigenvalues:

$$\mathrm{x}(t) = \sum_{j=0}^{+\infty} \phi_j(x(0))\tilde{\boldsymbol{\nu}}_j e^{(\rho_j + i\omega_j)t} \approx \mathrm{x}^{(k)} \doteq \sum_{j=0}^{m} \boldsymbol{\nu}_j \lambda_j^k, \tag{6}$$

where $\phi_j(x(0))$ is the Koopman eigenfunction and $\tilde{\boldsymbol{\nu}}_j$ is the Koopman mode, representing a complex-valued flow structure, associated with the growth rate ρ_j and frequency ω_j. Equivalently to (6), it is assumed that there exists a linear mapping F, describing the evolution of the the flow field in time: $\mathrm{x}^{(k+1)} = F\mathrm{x}^{(k)}$.

3.3. Balanced DMD. Following [36], we first collect $m+1$ snapshots of the state responses, of the full-order nonlinear system (3), which corresponds in this work to the finite element approximation of the incompressible Navier-Stokes equations, to a finite-amplitude impulsive input $\delta(t - t_0)$, $t_0 \geq 0$, and arrange them in two matrices: $X_{\mathrm{NL}} = [\mathrm{x}^{(0)}, ..., \mathrm{x}^{(m-1)}]$ and $Z_{\mathrm{NL}} = [\mathrm{x}^{(1)}, ..., \mathrm{x}^{(m)}]$. We then perform the reduced SVD of the matrix X_{NL}: $X_{\mathrm{NL}} = U\Sigma V^{\mathrm{T}}$, where $\Sigma \in \mathbb{R}^{m \times m}$ is diagonal, $U \in \mathbb{R}^{n \times m}$, $V \in \mathbb{R}^{m \times m}$ and $U^{\mathrm{T}}U = V^{\mathrm{T}}V = I_m$. Define the $m \times m$ matrix $\bar{F} = U^{\mathrm{T}}Z_{\mathrm{NL}}V\Sigma^{-1}$ whose eigendecomposition is given by $\bar{F}R = R\Lambda$, with $R = [r_1, ..., r_m]$ and $\Lambda = \mathrm{diag}(\lambda_1, ..., \lambda_m)$. The dynamic modes $\boldsymbol{\nu}_j$ are then given by $\Phi_m = [\boldsymbol{\nu}_1, ..., \boldsymbol{\nu}_m] = URD$, where D is a diagonal matrix, used to scale the modes, computed as in [5], so that the sum of the modes equals the first data vector $\mathrm{x}(t_0)$. If the snapshots are computed from a system with no inputs, it is assumed, as in [36], that the evolution of the flow field can be expressed by a linear map $F \in \mathbb{R}^{n \times n}$: $\mathrm{x}^{(k+1)} = F\mathrm{x}^{(k)}$. A least square approximation of the matrix F is given by $F = Z_{\mathrm{NL}}X_{\mathrm{NL}}^{\dagger} \approx Z_{\mathrm{NL}}V\Sigma^{-1}U^{\mathrm{T}}$, where $(\cdot)^{\dagger}$ denotes the Moore-Penrose pseudoinverse of $(\cdot)$, *i.e.*, $X_{\mathrm{NL}}^{\dagger} = [X_{\mathrm{NL}}X_{\mathrm{NL}}^{\mathrm{T}}]^{-1}X_{\mathrm{NL}}$.
In the case of a system with inputs, a linear system, approximating the nonlinear

one, can be obtained as follows:

$$\begin{cases} \mathrm{x}^{(k+1)} & \approx U\bar{F}U^{\mathrm{T}}\mathrm{x}^{(k)} + U\bar{G}\mathrm{v}^{(k)}, \\ \mathrm{y}^{(k)} & \approx \bar{H}U^{\mathrm{T}}\mathrm{x}^{(k)}, \end{cases} \tag{7}$$

where $\bar{G} = U^{\mathrm{T}}\mathrm{x}^{(0)} \in \mathbb{R}^m$ and $\bar{H} = CU \in \mathbb{R}^{1\times m}$. Note that the input vector $U\bar{G}$ is chosen as the projection of the excited initial condition $\mathrm{x}^{(0)}$ onto the POD basis, spanned by the columns of U. This choice is motivated by the fact that the impulse responses of system (7), needed to compute the balanced modes, can be expressed as $\mathrm{x}^{(k)} \approx F^k\mathrm{x}^{(0)} = U\bar{F}^kU^{\mathrm{T}}\mathrm{x}^{(0)}$.

In fluid systems, the dimension of the attractor is bounded, so that the essential dynamics is finite-dimensional, see [27]. Therefore, there cannot be any asymptotically growing structures and thus $\rho_j \leq 0$ for all $j = 0, ..., +\infty$, cf. [3]; *i.e.* all the Ritz values λ_j lie within the unit cycle. The so-obtained DMD linear model (7), is thus stable (*i.e.* $|\lambda_j| \leq 1$, $j = 1, ..., m$) but the dynamic properties of the attracting set are lost. Since limit cycles cannot be described using linear dynamics, a projection onto the asymptotically stable eigenspace is performed.

Let $L \in \mathbb{R}^m$ be the left eigenvector matrix of $\bar{F}$: $\bar{F}^{\mathrm{T}}L = L\Lambda^{\mathrm{H}}$, where $(\cdot)^{\mathrm{H}}$ denotes the Hermitian transpose of $(\cdot)$. The right and left eigenvectors are partitioned as $R = [R_s, R_u]$ and $L = [L_s, L_u]$, respectively, where the subscripts $_s$ and $_u$ refer to the parts of the spectrum Λ_s, which is asymptotically stable, and Λ_u, which lies on the unit circle, respectively. The projection operator $\mathbb{P}_s = I_m - R_u(L_u^{\mathrm{H}}R_u)^{-1}L_u^{\mathrm{H}}$, where I_m is the $m \times m$ identity matrix, is used to restrict the dynamics of (7) to the asymptotically stable subspace of $\bar{F}$. The balanced POD is computed using the full state (direct and adjoint) snapshots of the reduced *m-th* order projected system

$$\begin{cases} \bar{\mathrm{x}}_s^{(k+1)} & = \bar{F}\bar{\mathrm{x}}_s^{(k)} + \mathbb{P}_s\bar{G}\mathrm{v}^{(k)}, \\ \bar{\mathrm{y}}^{(k)} & = \bar{H}\mathbb{P}_s\bar{\mathrm{x}}_s^{(k)}, \end{cases} \tag{8}$$

where $\bar{\mathrm{x}}_s^{(k)} = \mathbb{P}_s\bar{\mathrm{x}}^{(k)} = \mathbb{P}_sU^{\mathrm{T}}\mathrm{x}^{(k)} \in \mathbb{R}^m$, in order to select the $r \ll m$ relevant modes to be retained in the reduced-order model. The full-order balanced-POD modes $\Phi = U\Phi_r, \quad \Psi = U\Psi_r$, with Φ_r, Ψ_r defined in (5), yield the asymptotically stable, linear model of order r:

$$\begin{cases} \xi^{(k+1)} & = \bar{A}\xi^{(k)} + \bar{B}\mathrm{v}^{(k)}, \\ \bar{\mathrm{y}}^{(k)} & \approx \bar{C}\xi^{(k)}, \end{cases} \tag{9}$$

where $\bar{A} = \Psi_r^{\mathrm{T}}\bar{F}\Phi_r$, $\bar{B} = \Psi_r^{\mathrm{T}}\bar{G}$ and $\bar{C} = \bar{H}\Phi_r$.

4. Regulating Control

For the specific application to flow separation control, the sampling time $k\Delta t$, used to construct the ROM is much smaller compared to the fluid time-scales. Therefore, the action of the discrete-time input $\mathrm{v}^{(k)}$ on the flow field can be considered continuous. The discrete-time ROM (9) can be thus converted into a continuous-time system ($\mathrm{w} \in \mathbb{R}$)

$$\begin{cases} \dot{\xi} & = A\xi + B\mathrm{v}, \quad \xi(0) = \xi_0, \\ \mathrm{y} & = C\xi, \end{cases} \tag{10}$$

where, $\xi : \mathbb{R} \to \mathbb{R}^r$ is the reduced-order state vector; $A \in \mathbb{R}^{r\times r}$ is a low-order linear operator approximating the nonlinear dynamics, whose eigenvalues belong to the open left half of the complex plane; $B \in \mathbb{R}^r$ is the input matrix; $C \in \mathbb{R}^{1\times r}$ is the

output matrix. Let I_r be the $r \times r$ identity matrix and $P(s) = C(sI - A)^{-1}B$, whose poles have all negative real part, be the open-loop transfer function of system (10). Define $P(s) \doteq \frac{n_P(s)}{d_P(s)}$ and let v^*, y^* and ξ^* be the references for the input, output and state, respectively. Denoting $\tilde{\xi} = \xi - \xi^*$ and $\eta = -\mathrm{v}^* : \mathbb{R} \to \mathbb{R}$, the error dynamics are given by

$$\begin{cases} \dot{\tilde{\xi}} &= A\tilde{\xi} + B(\mathrm{v} + \eta), \\ \dot{\eta} &= 0, \quad \eta(0) = \eta_0, \\ \tilde{\mathrm{y}} &= C\tilde{\xi}, \end{cases} \tag{11}$$

so that the control problem can be formulated as a disturbance rejection problem, where the reference input $\mathrm{v}^* = -\eta$ can be viewed as a disturbance vector, which matches the control input v, see [25].

Similarly to [24], the control problem becomes to design a suitable feedback law $\mathrm{v}(t)$ for system (10), based on the real-time measurement $\mathrm{y}(t)$, in order to robustly regulate the latter to a given reference region (*e.g.* $\mathrm{y}(t) \geq \epsilon > 0$). The key objective is to design v such that the closed-loop trajectories of system (3) are guaranteed to evolve within some "safe" invariant set in different scenarios, depending on uncertain parameters (*e.g.*, the Reynolds number Re and angle of attack β). However, as the linear ROM (10) is computed at given parameters (*i.e.* Re and β), it cannot give an accurate approximation of the full-order nonlinear dynamics (3) when the unknown parameters are varied. Furthermore, the dependence of dynamical properties of fluid systems on such parameters is highly nonlinear. Therefore, on the basis of the recent results in [25], we design a robust output regulator guaranteeing exponential convergence of the regulation error: it only requires the system to have a non-zero steady-state gain of known sign.

The uncertain matrices A, B, C, as well as the order of the model, highly depend on the uncertain set of parameters which defines the physical problem, such as, in our specific application, the Reynolds number Re and angle of attack β. Given a certain range for the uncertain parameters (*e.g.* Re and β), we only assume that there exist some positive constants r, $\epsilon_{a_{jk}}$, ϵ_{b_j} and ϵ_{c_j}, such that the coefficients of A, B, C, belong to their corresponding compact sets $[a_{jk} - \epsilon_{a_{jk}}, a_{jk} + \epsilon_{a_{jk}}]$, $[b_j - \epsilon_{b_j}, b_j + \epsilon_{b_j}]$, $[c_j - \epsilon_{c_j}, c_j + \epsilon_{c_j}]$, for any $j, k = 1, ..., r$, and are such that $P(0)$ does not change sign, within the whole range.

4.1. Control Algorithm: Robust Integrator. We translate the initial control objective (2) into the following: $\mathrm{y} \in \Omega_\epsilon = [\epsilon_m, \epsilon_M]$, where ϵ_m and ϵ_M are chosen positive constants. In particular, the lower bound for the output reference can be chosen in order to guarantee any a priori fixed requirement, such as, in the present application, the suppression of the separation bubble over the aerofoil; the upper bound can be chosen in order to limit the power consumption. Therefore, the control problem, similarly to [24], becomes to design v such that the chosen controlled output y belongs to a "safe" compact set Ω_ϵ.

In particular, the reference output y^* is chosen as

$$\mathrm{y}^*(t) = \begin{cases} \epsilon_m, & \text{if } \mathrm{y}(t) < \epsilon_m, \\ \mathrm{y}(t), & \text{if } \mathrm{y}(t) \in \Omega_\epsilon, \\ \epsilon_M, & \text{if } \mathrm{y}(t) > \epsilon_M. \end{cases} \tag{12}$$

The references for the state and the input are defined as

$$\xi^*(t) = \begin{cases} \xi_m, & \text{if } \mathrm{y}(t) < \epsilon_m, \\ \xi(t), & \text{if } \mathrm{y}(t) \in \Omega_\epsilon, \\ \xi_M, & \text{if } \mathrm{y}(t) > \epsilon_M, \end{cases} \tag{13}$$

$$\mathrm{v}^*(t) = \begin{cases} \mathrm{v}_m, & \text{if } \mathrm{y}(t) < \epsilon_m, \\ \operatorname{argmin}_{\bar{\mathrm{v}} \in \Omega_\eta} \left| \bar{\mathrm{v}} + \hat{\eta} \right|, & \text{if } \mathrm{y}(t) \in \Omega_\epsilon, \\ \mathrm{v}_M, & \text{if } \mathrm{y}(t) > \epsilon_M, \end{cases} \tag{14}$$

where the constant pairs ξ_m, v_m and ξ_M, v_M can be computed by solving the regulator problem, see [25], for $\mathrm{y}^* = \epsilon_m$ and $\mathrm{y}^* = \epsilon_M$, respectively.

The resulting control algorithm reads

$$\begin{cases} \dot{\hat{\eta}} & = k \operatorname{sign}(P(0)) \tilde{\mathrm{y}}, \quad \hat{\eta}(0) = \hat{\eta}_0, \\ \mathrm{v} & = -\hat{\eta}. \end{cases} \tag{15}$$

The overall feedback controller (15), (12) depends on: the measured output y; the bounded reference y^*; the known sign of $P(0)$; the positive design parameters k, ϵ_m, ϵ_M. Note that, when $\epsilon = \epsilon_m = \epsilon_M$, the control algorithm (15), (12) reduces to (15), with a constant output reference.

4.1.1. Stability Analysis. The main result of this section, which extends the results obtained in [25] to systems of the form (10), (15), (12), is summarised by the following theorem: it shows how a robust integral controller is sufficient to guarantee the solution of the slow separation problem for the reduced-model (10).

Theorem 1. *Consider the closed-loop system (10), (15), (12). Assume that* $P(0) \neq 0$ *with known sign. Then, for any initial condition* $(\xi_0, \eta_0, \hat{\eta}_0)$*, there exists a sufficiently small* $k^* > 0$ *such that the regulation error* $y(t) - y^*(t)$ *and the control input error* $v(t) - v^*(t)$ *exponentially tend to zero, as* t *tends to infinity, for any* $0 < k \leq k^*$*.*

Proof. a). Case $\epsilon = \epsilon_m = \epsilon_M$. System (11) can be rewritten as

$$\tilde{\mathrm{Y}}(s) = P(s) \left(\mathrm{v}(s) + \eta \right), \quad P(s) \doteq \frac{n_P(s)}{d_P(s)}. \tag{16}$$

The stability of the closed-loop system is determined by the zeros of the transfer function

$$Q(s) = 1 + kP(s) \left(\frac{\operatorname{sign}(P(0))}{s} \right) \doteq \frac{n_Q(s)}{d_Q(s)}. \tag{17}$$

By the root locus, for sufficiently small $k > 0$, r zeros of $Q(s)$ are sufficiently close to the r poles of $P(s)$ and, therefore, they have negative real part. The remaining branch of the root locus starts from 0 in the s-plane with angle π, so that also the remaining zeros of $Q(s)$ have negative real part.

b). Case $\epsilon_m < \epsilon_M$. Let $\tilde{\eta} = \mathrm{v} - \mathrm{v}^* = \eta - \hat{\eta}$ and $\tilde{\chi} = [\tilde{\xi}, \tilde{\eta}]^{\mathrm{T}}$. The closed-loop error dynamics can be written as

$$\begin{aligned} \dot{\tilde{\chi}} &= \begin{bmatrix} A & B \\ -k \operatorname{sign}(P(0)) C & 0 \end{bmatrix} \tilde{\chi} \doteq A_c \tilde{\chi}, \\ \tilde{\mathrm{y}} &= [C, 0] \, \tilde{\chi}. \end{aligned}$$

The characteristic polynomial of the closed-loop matrix A_c can be computed as

$$\begin{aligned} p_{A_c}(s) &= \det(sI_{r+1} - A_c) = \det \begin{bmatrix} sI_r - A & B \\ -k\ \mathrm{sign}(P(0))C & s \end{bmatrix} \\ &= \det(sI_r - A)\left(s + kC(sI_r - A)^{-1}B\mathrm{sign}(P(0))\right) \\ &= sd_P(s) + kn_P(s)\mathrm{sign}(P(0)) = n_Q(s). \end{aligned}$$

where I_{r+1} is the $(r+1) \times (r+1)$ identity matrix. Therefore, A_c is Hurwitz, as its eigenvalues coincide with roots of $n_Q(s)$ and have negative real part for any sufficiently small k. Thus, there exist two symmetric, positive definite matrices $\mathcal{P}$ and $\mathcal{Q}$ satisfying the Lyapunov equation: $\mathcal{P}A_c + A_c^{\mathrm{T}}\mathcal{P} = -\mathcal{Q}$. Consider the candidate Lyapunov function $\mathcal{V}(t) \doteq \tilde{\chi}^{\mathrm{T}}(t)\mathcal{P}\tilde{\chi}(t)$, satisfying

$$\alpha_1\|\tilde{\chi}(t)\|^2 \leq \mathcal{V}(t) \leq \alpha_2\|\tilde{\chi}(t)\|^2, \tag{18}$$

where $\alpha_1,\ \alpha_2 > 0$ are positive constants. The time derivative of $\mathcal{V}(t)$, along the trajectories of the closed-loop system satisfies the following inequality:

$$\dot{\mathcal{V}} \leq -\tilde{\chi}^{\mathrm{T}}\mathcal{Q}\tilde{\chi} + 2\tilde{\chi}^{\mathrm{T}}\mathcal{P}\zeta(\tilde{\chi}) \leq -\mathcal{M}\|\tilde{\chi}\|^2 \leq -\mathcal{M}\|\tilde{\chi}\|^2,$$

where $\mathcal{M} = \|\mathcal{Q}\|$. Therefore, there exists an $\alpha_3 > 0$ such that

$$\dot{\mathcal{V}} \leq -\alpha_3\|\tilde{\chi}\|^2 \leq -\frac{\alpha_3}{\alpha_2}\mathcal{V}, \tag{19}$$

thus implying the closed-loop boundedness and the exponential convergence to zero of both the regulation error $\tilde{\mathrm{y}}(t)$ and the control input error $\mathrm{v}(t) - \mathrm{v}^*$, as t tends to infinity.

Let $\tilde{\xi} = \xi - \xi^*$ and $\tilde{\eta} = \mathrm{v} - \mathrm{v}^*$. When the output vector belongs to the compact set Ω_ϵ, we have: $\tilde{\xi} \equiv 0$, $\dot{\tilde{\xi}} \equiv 0$, $\dot{\tilde{\eta}} \equiv 0$. Thus, for any $t \geq 0$ such that $\mathrm{y}(t) \in \Omega_\epsilon$, $\dot{\mathcal{V}}(t) \equiv 0$. When the output does not belong to the reference region, there exist three positive constants $\alpha_1,\ \alpha_2,\ \alpha_3 > 0$ such that $\mathcal{V}(t)$ and its time derivative satisfy (18) and (19), respectively. Therefore, for any $t \geq 0$ such that $\mathrm{y}(t) \notin \Omega_\epsilon$, $\dot{\mathcal{V}}(t) < 0$ and the distance $\mathrm{d}_{\mathcal{P}}(\chi(t), \Omega_\chi) \doteq \inf_{\bar{\chi}\in\Omega_\chi}\|\chi - \bar{\chi}\|_{\mathcal{P}} \doteq \sqrt{\tilde{\chi}^{\mathrm{T}}\mathcal{P}\tilde{\chi}}$,between χ and its reference set Ω_χ satisfies $\mathrm{d}^2_{\mathcal{P}}(\chi(t), \Omega_\chi) \leq \alpha_2\|\tilde{\chi}\|^2 \leq e^{-\alpha t}\delta$,where $\alpha = \alpha_3/\alpha_2$ and $\delta = \mathcal{V}(0)\alpha_2/\alpha_1$. Since $0 \leq \mathcal{V}(t) \in \mathcal{C}^1$ is lower bounded and its derivative is semi-negative definite, it admits a finite limit, see [13, p. 61]. Closed-loop boundedness and exponential convergence of $\dot{\mathcal{V}}(t)$ (and, therefore, of $\dot{\tilde{\xi}}$ and $\dot{\tilde{\eta}}$) to zero are thus guaranteed, according to Barbalats lemma, as $\mathcal{V}(t)$ is uniformly continuous. Consequently, $\xi(t)$ converges to a constant reference $\bar{\xi} \in \Omega_\xi$ and $\mathrm{v}(t)$ converges to a constant value $\bar{\mathrm{v}}$, as t tends to infinity. If $\bar{\mathrm{v}} \notin \Omega_\eta$, then $\bar{\mathrm{y}} = C\bar{\xi} = -P(0)\bar{\mathrm{v}} \notin \Omega_\epsilon$, which contradicts $\bar{\xi} \in \Omega_\xi$. Therefore, $\bar{\mathrm{v}} \in \Omega_\eta$ and the distance $\mathrm{d}_{\mathcal{P}}(\chi(t), \Omega_\chi)$ exponentially tends to zero, as t tends to infinity. □

4.2. Control Algorithm: Time-Varying Gain. A variant of (15) is proposed here in order to extend the designed controller to a wider class of closed-loop systems. Define

$$\begin{cases} \dot{\hat{\eta}} &= k\ \mathrm{sign}(P(0))\tilde{\mathrm{y}} - \mu\hat{\eta}\tilde{\mathrm{y}}^2, \quad \hat{\eta}(0) = \hat{\eta}_0, \\ \mathrm{v} &= -\sigma(\mathrm{y})\hat{\eta}, \end{cases} \tag{20}$$

where $k > 0$ and $\mu \geq 0$ are chosen control gains and $0 < \sigma(\mathrm{y}) \leq 1$ is any real-valued, bounded, continuous function. In particular, similarly to the projection algorithm

defined in [26], $\sigma(\mathrm{y})$ is chosen as

$$\sigma(\mathrm{y}) = \begin{cases} 1 & \text{if } \mathrm{y} < \epsilon_m \text{ or } \hat{\mathrm{v}}^* < 0, \\ 1 - \sigma_\epsilon(\mathrm{y}) & \text{if } \mathrm{y} \in \Omega_\epsilon \text{ and } \hat{\mathrm{v}}^* > 0, \\ 1 - \sigma_\epsilon(\epsilon_M) & \text{if } \mathrm{y} > \epsilon_M \text{ and } \hat{\mathrm{v}}^* > 0, \end{cases} \tag{21}$$

$$\sigma_\epsilon(\mathrm{y}) = \frac{\mathrm{y}^2 - \epsilon_m^2}{\mathrm{y}_M^2 - \epsilon_m^2}, \tag{22}$$

where $\mathrm{y}_M > \epsilon_M \geq \epsilon_m > 0$ are positive design parameters. Note that, when $\epsilon = \epsilon_m = \epsilon_M$, the control algorithm (12), (20), (21), (22) reduces to (15), with a constant output reference.

Remark 1. The introduction of the function $\sigma(\mathrm{y})$ is used, for this specific application, to reduce the control action, once the controlled output reaches the desired region. This time-varying gain, along with the less restrictive reference signal, allows for the use of higher gains k, thus leading to faster dynamic performances, whilst limiting the overshoot.

Remark 2. The anti-windup term $\mu\hat{\eta}\tilde{\mathrm{y}}^2$ plays a stabilizing role similar to the one played by the well-known term $\mu\hat{\eta}$, where the quadratic function of the tracking error $\tilde{\mathrm{y}}^2$ has been introduced in order not to affect the stability analysis, when μ is sufficiently small.

Theorem 2. *Consider the closed-loop system (10), (12), (20), (21), (22). Assume that $P(0) \neq 0$ with known sign. Then, for any initial condition $(\xi_0, \eta_0, \hat{\eta}_0)$, there exist a $k^* > 0$ and a sufficiently small $\mu^* \geq 0$, depending on k^*, such that the regulation error $\tilde{y}(t)$ and the control input error $v(t) - v^*$ exponentially tend to zero, as t tends to infinity, for any $0 < k \leq k^*$, $0 \leq \mu \leq \mu^*$.*

Proof. *a*). Case $\sigma(t) \equiv 1$. The closed-loop error dynamics can be written as

$$\begin{aligned} \dot{\tilde{\chi}} &= \begin{bmatrix} A & B \\ -k\ \mathrm{sign}(P(0))C & 0 \end{bmatrix} \tilde{\chi} + \begin{bmatrix} 0 \\ \mu\tilde{\xi}^{\mathrm{T}} C^{\mathrm{T}} C \tilde{\xi}(\eta - \tilde{\eta}) \end{bmatrix} \doteq A_c\tilde{\chi} + \zeta(\tilde{\chi}), \\ \tilde{\mathrm{y}} &= [C, 0]\, \tilde{\chi}, \end{aligned}$$

where A_c is Hurwitz for any sufficiently small k. Thus, there exist two symmetric, positive definite matrices $\mathcal{P}$ and $\mathcal{Q}$ satisfying the Lyapunov equation: $\mathcal{P}A_c + A_c^{\mathrm{T}}\mathcal{P} = -\mathcal{Q}$. Consider the candidate Lyapunov function $\mathcal{V}(t) = \tilde{\chi}^{\mathrm{T}}(t)\mathcal{P}\tilde{\chi}(t)$, satisfying (18). The time derivative of $\mathcal{V}(t)$, along the trajectories of the closed-loop system satisfies the following inequality:

$$\begin{aligned} \dot{\mathcal{V}} &\leq -\tilde{\chi}^{\mathrm{T}}\mathcal{Q}\tilde{\chi} + 2\tilde{\chi}^{\mathrm{T}}\mathcal{P}\zeta(\tilde{\chi}) \leq -\mathcal{M}_1\|\tilde{\chi}\|^2 + 2\mathcal{M}_2\mu\|\tilde{\chi}\|^2 \left|\eta\tilde{\eta} - \tilde{\eta}^2\right| \\ &\leq -\left(\mathcal{M}_1 - \frac{\mathcal{M}_2\mu\eta^2}{2}\right)\|\tilde{\chi}\|^2, \end{aligned}$$

where $\mathcal{M}_1 = \|\mathcal{Q}\|$, $\mathcal{M}_2 = \|\mathcal{P}\|\|C\|^2$. Therefore, for sufficiently small μ, there exists an $\alpha_3 > 0$ such that (19) is satisfied, thus implying the closed-loop boundedness and the exponential convergence to zero of both the regulation error $\tilde{\mathrm{y}}(t)$ and the control input error $\mathrm{v}(t) - \mathrm{v}^*$, as t tends to infinity.

b). Case with time-varying $\sigma(t)$. When the output does not belong to the reference region, the closed-loop error dynamics becomes

$$\dot{\tilde{\chi}} = \begin{bmatrix} A & B \\ -k\sigma(\mathrm{y})\mathrm{sign}(P(0))C & 0 \end{bmatrix} \tilde{\chi} + \begin{bmatrix} 0 \\ \mu\tilde{\xi}^{\mathrm{T}} C^{\mathrm{T}} C\tilde{\xi}(\eta - \tilde{\eta}) \end{bmatrix} \doteq A_\sigma \tilde{\chi} + \zeta(\tilde{\chi}),$$
$$\tilde{\mathrm{y}} = [C, 0]\, \tilde{\chi},$$

so that, since $k\sigma(\epsilon_M) \leq k\sigma(\mathrm{y}) \leq k$, A_σ is Hurwitz for sufficiently small k and Theorem 1 holds. Furthermore, there are no solutions on the imaginary axis of the equation

$$1 + K_\sigma(s)P(s)\frac{1}{s} = 0,$$

where $K_\sigma(s) > 0$ is the Laplace transform of $k\sigma(\epsilon_M) < k\sigma(\mathrm{y}(t)) \leq k$, for any finite $K_\sigma(s)$, so that the positive root locus cannot cross the imaginary axis. □

5. A Practical Application: Flow Separation Control

We propose the application of both the model reduction method, described in section 3, and the regulating control, described in section 4, to the unsteady incompressible Navier-Stokes equations, in the presence of a body force distribution generated by the plasma actuator. The application case considered here is the suppression of the recirculating bubble on the suction side of a NACA-0012 profile at different, but fixed, Reynolds numbers and angles of attack.

5.1. Physical Model. Let Ω be an open bounded domain in $\mathbb{R}^2$ and let $T > 0$ denote the final time. The flow of an incompressible viscous Newtonian fluid can be described by the non-dimensionalised Navier-Stokes equations, which are derived from the conservation of mass and momentum, namely,

$$\begin{aligned} \partial_t \boldsymbol{u} &= -(\boldsymbol{u}\cdot\nabla)\boldsymbol{u} - \nabla p + \tfrac{1}{Re}\Delta\boldsymbol{u} + \boldsymbol{f} && \text{in } (0,T]\times\Omega, \\ 0 &= \nabla\cdot\boldsymbol{u} && \text{in } (0,T]\times\Omega, \end{aligned} \tag{23}$$

with initial condition

$$\boldsymbol{u}(0,\boldsymbol{x}) = \boldsymbol{u}_0(\boldsymbol{x}) \quad \text{in} \quad \Omega, \tag{24}$$

and boundary conditions

$$\begin{aligned} \boldsymbol{u}(t,\boldsymbol{x}) &= \boldsymbol{g}(\boldsymbol{x}) && \text{on } \Gamma_{\text{in}}, \\ \boldsymbol{u}(t,\boldsymbol{x}) &= 0 && \text{on } \Gamma_0, \\ (\tfrac{1}{Re}\nabla\boldsymbol{u} - pI)\boldsymbol{n} &= 0 && \text{on } \Gamma_{\text{out}}. \end{aligned} \tag{25}$$

Here: $\boldsymbol{x} \in \Omega$; $\boldsymbol{n}$ denotes the unit outward normal vector on $\partial\Omega = \Gamma_{\text{in}} \cup \Gamma_0 \cup \Gamma_{\text{out}}$; Γ_{in}, Γ_{out} and Γ_0 denote the inflow, outflow and wall boundaries, respectively; $\boldsymbol{u} : [0,T]\times\Omega \to \mathbb{R}^2$ is the velocity vector; $p : [0,T]\times\Omega \to \mathbb{R}$ is the pressure; $I \in \mathbb{R}^{2\times 2}$ is the identity matrix; $Re = \rho U_\infty c/\mu$ is the Reynolds number; U_∞ is the free-stream velocity (in m/s); ρ is the fluid density (in kg/m^3); $c = 0.1$m is the chord length, μ is the dynamic viscosity (in kg/(m·s)); $\boldsymbol{f} : [0,T]\times\Omega \to \mathbb{R}^2$ is the localised body force vector field, which represents the control input. The latter can be expressed as $\boldsymbol{f}(t,\boldsymbol{x}) = c/\rho U_\infty^2 (f_x(t,\boldsymbol{x}), f_y(t,\boldsymbol{x}))$, where f_x, f_y are the streamwise and normal component (in N/m^3). All the above listed functions are assumed to be sufficiently smooth. The wall-tangential velocity, evaluated at the selected sensor location $\boldsymbol{x}_P$,

$$\mathrm{y}(t) = u_\tau(t,\boldsymbol{x}_P) = \boldsymbol{\tau}(\boldsymbol{x_P})\cdot\boldsymbol{u}(t,\boldsymbol{x}_P), \tag{26}$$

where $\boldsymbol{\tau}$ denotes the tangent unit vector, is chosen as the measured output. The time scale disparity between the flow and the discharge frequencies allows for assuming that the force acts on the neutral fluid in a quasi-steady manner. The body force felt by the neutral flow is equivalent to the Lorentz force acting on the net charge density. Several models for the DBD actuator force have been proposed (see, for instance, [12] for a detailed review). The bilinear model proposed in [38] is widely used in the flow control literature, see, for instance, [9], because of its simplicity. The variation in space of the electric field, which is directly proportional to the Lorentz force, is linearised, without computing the detailed electric field. This assumption is not consistent with experiments, see, for instance, [14, 32], which show an exponential spatial decay. As a result, the model over-predicts the actuator effect. Here we select a modified version of the recent model proposed in [40], which demonstrated good agreement with the experimental data. The model is characterised by an exponential dependence on the spatial coordinates and, in particular, the force is modelled by a Rayleigh distribution, see [40]; thereby,

$$\boldsymbol{f}(t,\boldsymbol{x}) = f_\tau(t,x_\tau,y_n)\boldsymbol{\tau}(\boldsymbol{x}) + f_n(t,x_\tau,y_n)\boldsymbol{n}(\boldsymbol{x}) = I(t)\frac{\lambda_f x_\tau}{\sigma_f^2}e^{-x_\tau^2/2\sigma_f^2-\lambda_f y_n}\boldsymbol{\tau}(\boldsymbol{x}),$$

where, $I(t) = k_v \mathrm{V}(t)/\mathrm{V}_m$ ($k_v \in \mathbb{R}$, $\mathrm{V}_m = 1$ kV) is the total plasma force; $\mathrm{V}(t) : \mathbb{R} \to \mathbb{R}$ is the amplitude variation of the operation voltage (in kV); $\mathrm{v}(t) = \mathrm{V}(t)/\mathrm{V}_m$ is the corresponding non-dimensionalised voltage input, scaled by V_m; f_τ, f_n (in $\mathrm{N/m^3}$) are the tangential and normal components, with respect to the aerofoil, of the force density, respectively; $x_\tau, y_n \geq 0$ are related to $\boldsymbol{x} = (x, y)$ by a coordinate transformation and respectively refer to the tangent and normal components, relative to the geometry. The parameters $\lambda_f = 1.6$, $\sigma_f = 1.9$, $k_v = 5200e^{1/2}\sigma_f/\lambda_f$ are chosen as in [40], where this model has been compared with particle image velocimetry (PIV) data, whilst, for sake of simplicity, a simple linear dependence of the body force on the applied peak-to-peak voltage is assumed here.

5.2. Finite Element Approximation. The considered two-dimensional configuration is a NACA 0012 aerofoil geometry, denoted by Γ_N, in a rectangular channel $\Gamma_R \doteq \Gamma_{\text{in}} \cup \Gamma_R^+ \cup \Gamma_R^- \cup \Gamma_{\text{out}} = [0,10] \times [-2,2]$. Here, the wall boundary is $\Gamma_0 = \Gamma_N \cup \Gamma_R^+ \cup \Gamma_R^-$, where Γ_R^+ and Γ_R^- are the upper and lower walls of the channel, respectively. The inflow boundary condition on Γ_{in} is a parabolic velocity profile

$$\boldsymbol{g}(\boldsymbol{x}) = -\frac{4U_m}{h_c^2}\left(y^2 - \frac{h_c^2}{4}\right), \tag{27}$$

where $h_c = 4$ is the channel height and $U_m = 1$ is the maximum, non-dimensionalised inflow velocity. The full-order, nonlinear state-space system is be obtained by spatially discretising the system of nonlinear PDEs (23), (25), (24), (26), using a continuous Galerkin finite element method, thus yielding a nonlinear system of n ODEs,

$$\begin{cases} E\dot{\mathrm{x}} &= \mathcal{F}(\mathrm{x}) + G\mathrm{v} \qquad \text{in} \quad (0,T], \\ \mathrm{y} &= H\mathrm{x} \qquad\qquad\ \ \text{in} \quad (0,T], \end{cases} \tag{28}$$

with initial conditions

$$\mathrm{x}(0) = \mathrm{x}_0, \tag{29}$$

of the same form of (3), where, $\mathrm{x} = \mathrm{x}(t) : \mathbb{R} \to \mathbb{R}^n$ is the state vector representing the evolution in time of the nodal values of the flow fields; $\dot{\mathrm{x}} = \mathrm{d}\mathrm{x}/\mathrm{d}t$; $E \in \mathbb{R}^{n\times n}$ is related to the mass matrix; $\mathcal{F}(\cdot) : \mathbb{R}^n \to \mathbb{R}^n$ is a sufficiently smooth nonlinear function; $G \in \mathbb{R}^{n\times p}$ is the input matrix representing the nodal values of the time-independent part of the body force; $\mathrm{v} = \mathrm{v}(t) : \mathbb{R} \to \mathbb{R}^p$ is the input voltage; $\mathrm{y} = \mathrm{y}(t) : \mathbb{R} \to \mathbb{R}^q$ is the chosen control output; $H \in \mathbb{R}^{q\times n}$ is the output matrix representing the space-discretisation of (26). Quadratic and linear Lagrange polynomials are used for the velocity and pressure fields, respectively. An implicit, first-order backward Euler scheme is used for the time-discretisation. The FEniCS Python library, see [21], is used to implement the finite element method for the automatic generation of a fast, parallelized C++ code with the aim of performing accurate numerical simulations. The computational grid is generated using Triangle, see [37]. Note that the number n of states of system (28) is large ($\approx 10^4/10^6$) and depends on the grid resolution.

6. Simulation Results

The reduced-order DMD model (8) has been obtained from $m = 745$ snapshots of the state responses of system (28) to an impulsive input $\delta(t - t_0)$. The input is centred at $t_0 = 0.2$, with amplitude $\Delta\mathrm{v} = 2/\Delta t$, which was chosen so that $\delta(t - t_0)$ has unitary integral. The snapshots are taken every $20\Delta t$, where $\Delta t = 0.002$ is the simulation time-step, until the trajectories of the system approach a periodic orbit. The considered two-dimensional configuration, which is used to build the ROM, is the flow around a NACA 0012 aerofoil, with angle of attack $\beta = 20^\circ$ and $Re = 1000$. The sensor was placed at $2c/5$ and the actuator at $c/5$, corresponding to $x_\tau, y_n = 0$, where c is the chord length (see Figure 1). Accurate finite element simulations

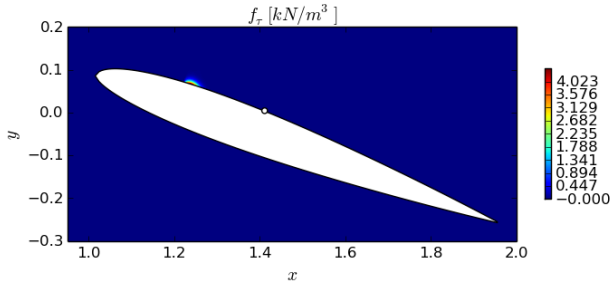

FIGURE 1. Actuator force density and sensor position.

have been performed, as described in Section 5.2, to compute the snapshots of the flow past the aerofoil. The dimension of the full-order system (28), describing the evolution in time of the two components of the fluid velocity, is $n \approx 2 \times 48000$, where 48000 is the number of elements in the unstructured grid. The balanced POD has been then computed using the direct and adjoint impulse responses of system (8), yielding a linear system with a positive steady-state gain: $\mathrm{sign}P(0) = 1$. The order r of the ROM is chosen so that $\sum_{i=1}^{r} \sigma_i / \sum_{i=1}^{r1} \sigma_i = 99\%$, where σ_i are the Hankel singular values defined in section 3.1, thus yielding the reduced-order, stable, balanced DMD model (9) of order $r = 11$, which is both controllable and observable.

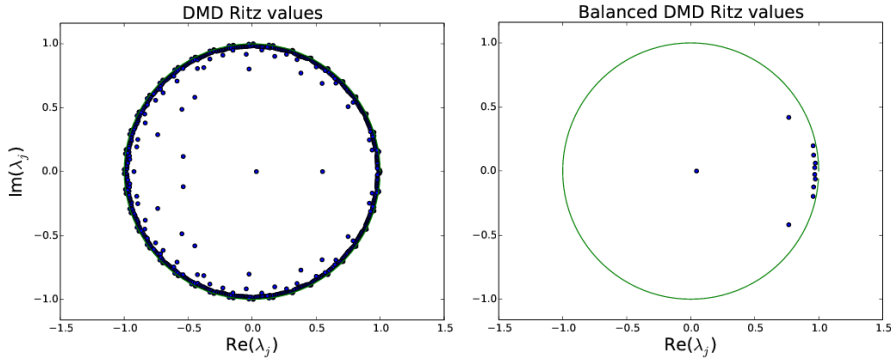

FIGURE 2. DMD (left) and balanced DMD (right) Ritz values $Re = 1000$, $\beta = 20°$.

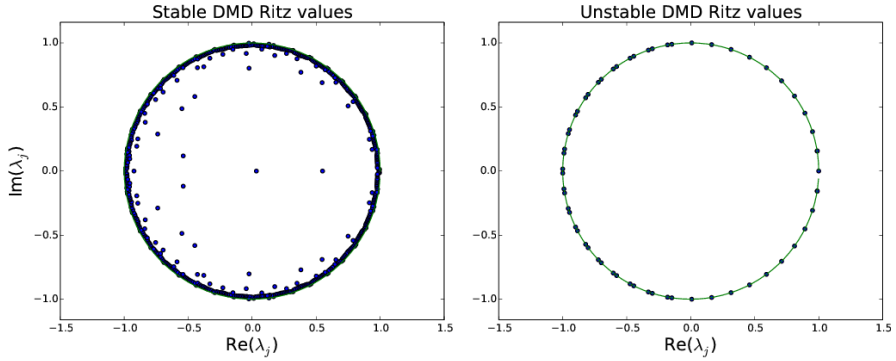

FIGURE 3. Stable (left) and unstable (right) Ritz values $Re = 1000$, $\beta = 20°$.

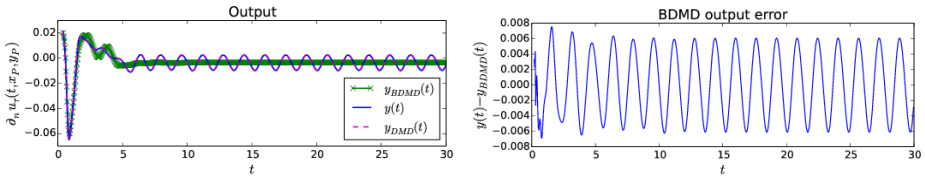

FIGURE 4. Balanced DMD (green), DMD (magenta) and full-order (blue) output responses to impulsive input (left) and balanced DMD output reconstruction error (right), for $t \geq 0.2$, $Re = 1000$, $\beta = 20°$.

Figure 2 shows the Ritz values computed by the DMD (left) and the proposed balanced DMD (right). Figure 3 shows the unstable (left) and stable (right) DMD Ritz values. The tails of the impulse responses of the full-order system (in blue) are compared in Figure 4 with the reconstructed outputs of the DMD (in magenta), and the balanced DMD (in green) models. An effective reconstruction of the full-order output dynamics is obtained, by retaining only $r = 11$ modes in the ROM

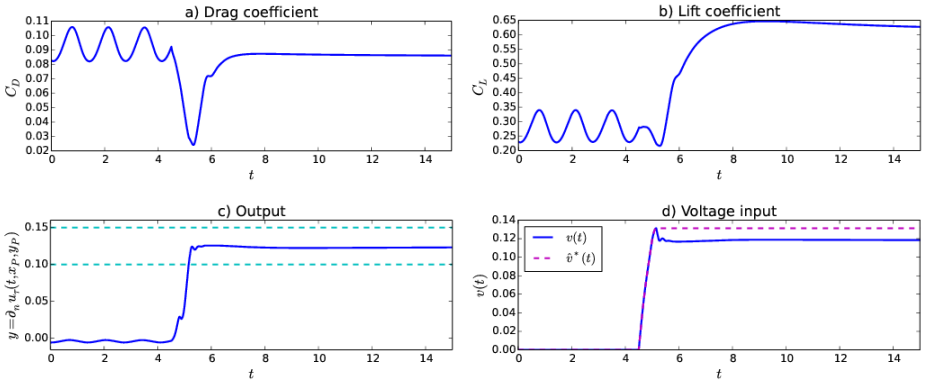

FIGURE 5. Simulation results for $Re = 1000$, $\beta = 15°$.

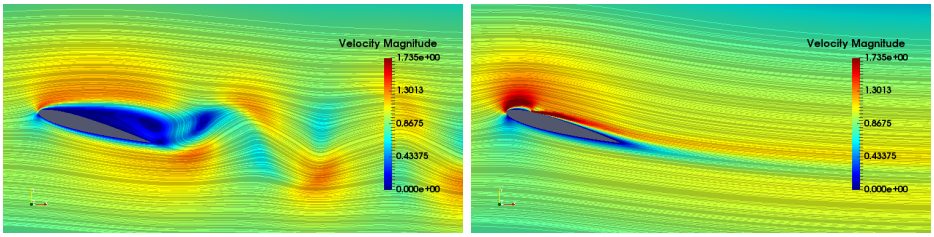

FIGURE 6. Snapshots of the velocity magnitude contours and streamlines, for $Re = 1000$, $\beta = 15°$, before the controller is turned on (top) and at $t = 15$ (bottom).

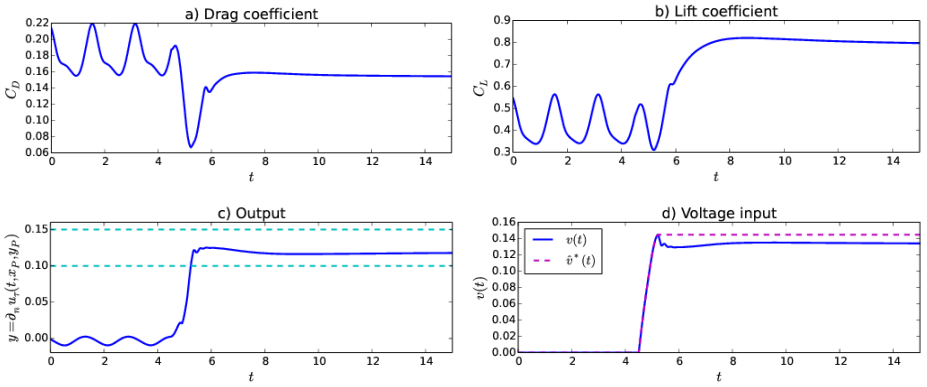

FIGURE 7. Simulation results for $Re = 1000$, $\beta = 20°$.

and with the additional advantage, with respect to system-identification methods, of retaining physical meaning in the ROM. Although the model well approximates the flow dynamics for $Re = 1000$, $\beta = 20°$, it is not guaranteed to be a good approximation of the full-order, nonlinear dynamics when the parameters vary. The robustness of the proposed control scheme (12), (20), (21), (22), which is

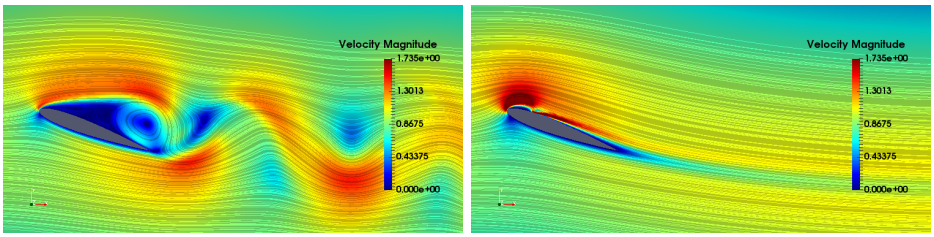

FIGURE 8. Snapshots of the velocity magnitude contours and streamlines, for $Re = 1000$, $\beta = 20°$, before the controller is turned on (left) and at $t = 15$ (right).

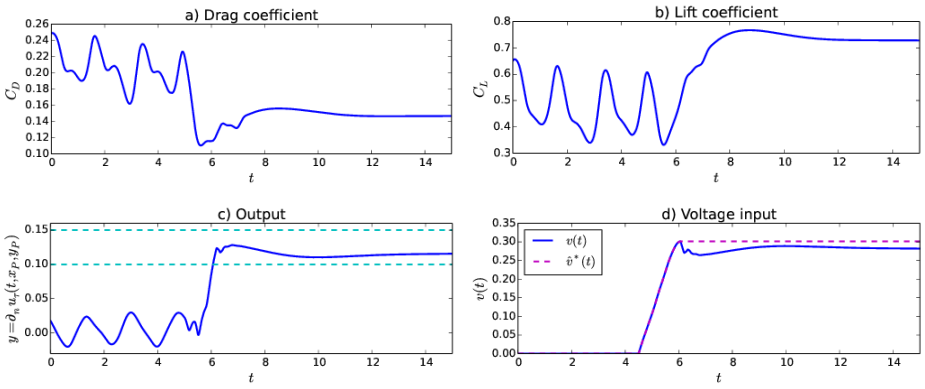

FIGURE 9. Simulation results for $Re = 2000$, $\beta = 20°$.

based on the constructed ROM, is thus tested in four different scenarios and both Reynolds number and angle of attack are varied: $Re = 1000$, $\beta = 15°$; $Re = 1000$, $\beta = 20°$; $Re = 2000$, $\beta = 20°$; $Re = 5000$, $\beta = 15°$. The control parameters are the same for the four cases and are chosen as: $k = 3$, $\mu = 10k$, $\epsilon_m = 0.1$, $\epsilon_M = 0.15$, $y_M = \epsilon_m + \epsilon_M$. The controller is turned on at $t = 4.5$. All the controller initial conditions are set to zero, whilst the initial velocity $\boldsymbol{u}$ and pressure fields p are in the limit cycle regime. Figures 5, 6 show the simulation results for $Re = 1000$, $\beta = 15°$. The snapshots of the velocity magnitude contours and streamlines in figure 6 show an evident flow reattachment: the proposed adaptive control effectively suppressed the separation bubble, as well as the shedding vortices. Both a significant increase of the lift coefficient (figure 5b), as well as a reduction of the drag coefficient (figure 5a), are achieved. A fast and smooth output regulation to $y^* \in \Omega_\epsilon$ is shown in figure 5c. The scaled, non-dimensionalised voltage input $\mathrm{v}(t) = \sigma(\mathrm{y})\hat{\mathrm{v}}^*(t)$ is shown in figure 5d, along with its corresponding estimated reference input $\hat{\mathrm{v}}^*(t)$. The same considerations hold for the simulation results at both $Re = 1000$, $\beta = 20°$ (depicted in figures 7, 8), $Re = 2000$, $\beta = 20°$ (depicted in figures 9, 10) and $Re = 5000$, $\beta = 15°$ (depicted in figures 11, 12). Note that, although a simple linear model, built upon a single scenario, is used for the control design, good dynamic performances are achieved as both the flow and geometry parameters are varied.

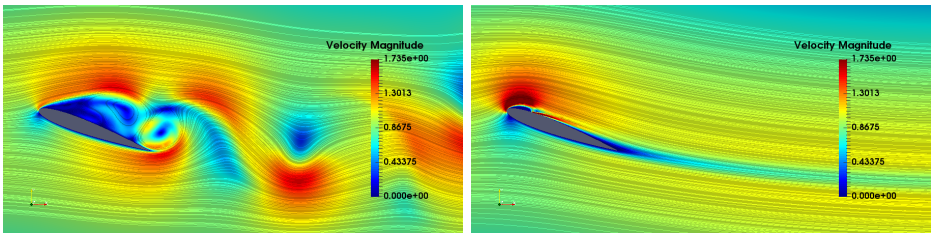

FIGURE 10. Snapshots of the velocity magnitude contours and streamlines, for $Re = 2000$, $\beta = 20°$, before the controller is turned on (left) and at $t = 15$ (right).

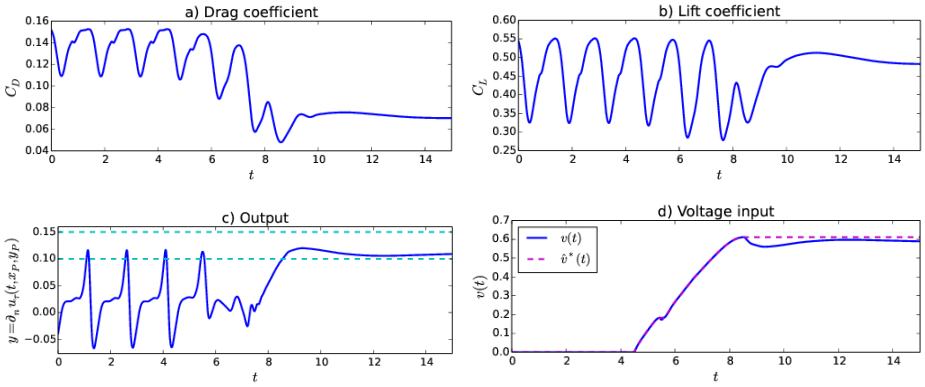

FIGURE 11. Simulation results for $Re = 5000$, $\beta = 15°$.

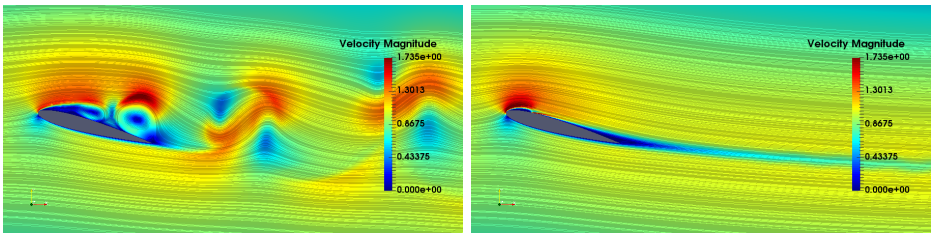

FIGURE 12. Snapshots of the velocity magnitude contours and streamlines, for $Re = 5000$, $\beta = 15°$, before the controller is turned on (left) and at $t = 15$ (right).

7. Conclusions

A low-order, control-oriented, linear model of unsteady flows past an aerofoil, in the presence of a DBD body force, is obtained using the snapshots of 2D finite element simulations at $Re = 1,000$. On the basis of the proposed model, a robust set-point tracking feedback controller has been designed: it guarantees exponential flow separation suppression when the steady-state gain of the approximated linear model is non-zero and of known sign. A simple configuration, with one sensor and one actuator is considered. Accurate 2D finite element simulations show that a fast flow reattachment is achieved, along with both stabilisation and increase/reduction

of the lift/drag, respectively. Although the proposed controller is simple, it is able to effectively suppress the separation bubble, as well as the shedding vortices, while achieving good dynamic performances, as both the Reynolds number and the angle of attack are varied. Furthermore, the presented method provides a criterion for optimising the placement of sensors and actuators: the problem of choosing both measurements and actuation can be addressed by selecting suitable configurations, leading to a non-zero steady-state gain of the approximated transfer function. Note that the chosen output can be experimentally measured by appropriate sensors and the extension of the proposed approach to 3D configurations is straightforward.

Acknowledgements

The research leading to these results has received funding from the People Programme (Marie Curie Actions) of the European Unions Seventh Framework Programme (FP7/2007-2013) under REA grant agreement no 608322.

References

[1] S. Ahuja and C. W. Rowley. Feedback control of unstable steady states of flow past a flat plate using reduced-order estimators. *J. Fluid Mech.*, 645:447–478, 2010.

[2] J. Annoni and P. Seiler. A method to construct reduced-order parameter varying models. *Int. J. Robust. Nonlin. Control*, 00:1–30, 2015.

[3] S. Bagheri. Koopman-mode decomposition of the cylinder wake. *J. Fluid Mech.*, 726:596–623, 2013.

[4] A. Barbagallo, D. Sipp, and P. J. Schmid. Closed-loop control of an open cavity flow using reduced-order models. *J. Fluid Mech.*, 641:1–50, 2009.

[5] B. A. Belson, J. H. Tu, and C. W. Rowley. Algorithm 945: `modred`-a parallelized model reduction library. *ACM Transactions on Mathematical Software*, 40(4):30, 2014.

[6] N. Benard and E. Moreau. Plasma flow control - autonomous lift improvement by slope-seeking. *AIAA paper*, 2009:4182, 2009.

[7] R. Broglia, D. Durante, and L. Pasuqale. Robust feedback control of two and three dimensional flow separation around a naca0012 profile using plasma actuators. In *DLES 11, Workshop on Drirect and Large Eddy Simulation*, Pisa, Italy, May 2017.

[8] L. Cattafesta and M. Sheplak. Actuators for active flow control. *Ann. Rev. Fluid Mech.*, 43:247–272, 2011.

[9] Y. C. Cho and W. Shyy. Adaptive flow control of low-reynolds number aerodynamics using dielectric barrier discharge actuator. *Progress in Aerospace Sciences*, 47:495–521, 2011.

[10] K.-S. Choi, T. N. Jukes, and R. D. Whalley. Turbulent boundary-layer control with plasma actuators. *Phil. Trans. R. Soc. A*, 369:1443–1458, 2011.

[11] S. S. Collis and R. D. Joslin. Issues in active flow control: theory, control, simulation, and experiment. *Progress in Aerospace Sciences*, 40:237–289, 2004.

[12] T. C. Corke, C. L. Enloe, and S. P. Wilkinson. Sdbd plasma enhanced aerodynamics: concepts, optimization and applications. *Progress in Aerospace Sciences*, 43:193–217, 2007.

[13] R. Courant. *Differential and Integral Calculus*, volume I. Blackie and Son, 1937.

[14] C. L. Enloe, T. E. McLaughlin, R. D. V. Dyken, K. D. Kachner, E. J. Jumper, and T. C. Corke. Mechanisms and responses of a single dielectric barrier plasma actuator: plasma morphology. *AIAA J.*, 42(3):589–594, 2004.

[15] R. E. Hanson, K. M. Bade, B. A. Belson, P. Lavoie, A. M. Naguib, and C. W. Rowley. Feedback control of slowly-varying transient growth by an array of plasma actuators. *Physics of Fluids*, 26:024102, 2014.

[16] M. Ilak and C. W. Rowley. Modeling of transitional channel flow using balanced proper orthogonal decomposition. *Physics of Fluids*, 20(3):034103, 2008.

[17] J. N. Juang and R. S. Pappa. An eigensystem realization algorithm for modal parameter identification and model reduction. *J. Guidance Control and Dynamics*, 8(5):620–627, 1985.

[18] J. Kim and T. R. Bewley. A linear systems approach to flow control. *Ann. Rev. Fluid Dynamics*, 39:383–417, 2007.

[19] B. O. Koopman. Hamiltonian systems and transformation in hilbert space. *Proceedings of the National Academy of Sciences*, 17(5):315–318, 1931.

[20] S. Lall, J. E. Marsden, and S. Glavaski. A subspace approach to balanced truncation for model reduction of nonlinear systems. *Int. J. Robust. Nonlin. Control*, 12:519–535, 2002.

[21] A. Logg, K.-A. Mardal, and G. N. Wells. Automated Solution of Differential Equations by the Finite Element Method. In *Lecture Notes in Computational Science and Engineering*. Springer, 2012.

[22] J. L. Lumley. The structure of inhomogeneous turbulence. *Atmospheric Turbulence and Wave Propagation*, 12:166–178, 1967.

[23] Z. Ma, S. Ahuja, and C. W. Rowley. Reduced-order models for control of fluids using the eigensystem realization algorithm. *Theoretical Comp. Fluid Dynamics*, 25:233–247, 2011.

[24] R. Marino, L. Pasquale, S. Scalzi, and C. M. Verrelli. Automatic rotor speed reference generator for electric vehicles under slip constraints. *IEEE Trans. on Intelligent Transportation Systems*, 16(6):3473–3478, 2015.

[25] R. Marino and P. Tomei. Output regulation for unknown stable linear systems. *Automatica*, 60(8):2213–2218, 2015.

[26] R. Marino, P. Tomei, and C. M. Verrelli. An adaptive tracking control from current measurements for induction motors with uncertain load torque and rotor resistance. *Automatica*, 44(10):2593–2599, 2008.

[27] I. Mezić. Spectral properties of dynamical systems, model reduction and decompositions. *J. Nonlin. Dyn.*, 41:309–325, 2005.

[28] I. Mezić. Analysis of fluid flows via spectral properties of the koopman operator. *Ann. Rev. Fluid Mech.*, 45:357–378, 2013.

[29] I. Mezić and A. Banaszuk. Comparison of systems with complex behaviour. *Physica*, 197:101–133, 2004.

[30] B. C. Moore. Principal component analysis in linear systems: controllability, observability, and model reduction. *IEEE Trans. on Automatic Control*, AC(1), 1981.

[31] E. Moreau. Airflow control by non-thermal plasma actuators. *J. Phys. D: App. Phys.*, 40:605–636, 2007.

[32] D. Orlov, T. Corke, and M. Patel. Electric circuit model for aerodynamic plasma actuator. *AIAA paper*, 1206:2006, 2006.

[33] L. Pasquale. *Robust feedback control of flow separation using plasma actuators.* PhD thesis, Department of Electrical and Electronic Engineering. Faculty of Engineering, The University of Nottingham (UK), 2017.

[34] C. W. Rowley. Model reduction for fluids, using balanced proper orthogonal decomposition. *Int. J. of Bifurcation and Chaos*, 15(03):997–1013, 2005.

[35] C. W. Rowley and I. Mezić. Spectral analysis of nonlinear flows. *J. Fluid Mech.*, 641:115–127, 2009.

[36] P. J. Schmid. Dynamic mode decomposition of numerical and experimental data. *Int. J. Control*, 656:5–28, 2010.

[37] J. R. Shewchuk. Delaunay refinement algorithms for triangular mesh generation. *Comp. Geometry*, 47(7):741–778, 2002.

[38] W. Shyy, B. Jayaraman, and A. Andersson. Modeling of glow discharge-induced fluid dynamics. *J. of App. Physics*, 92(11):6434, 2002.

[39] J. J. Wang, K.-S. Choi, L. H. Feng, T. N. Jukes, and R. D. Whalley. Recent developments in dbd plasma flow control. *Progress in Aerospace Sciences*, 62:52–78, 2013.

[40] Q. Yang and Y. M. Chung. Numerical study of reducing turbulent skin-friction drag using dmd plasma actuators. *EDRFCM 2015*, page Cambridge, 2015.

[41] K. Zhou, G. Salomon, and E. Wu. Balanced realization and model reduction for unstable systems. *Int. J. Robust. Nonlin. Control*, 3:183–198, 1999.

CNR-INSEAN - Marine Technology Research Institute, Via di Vallerano 139, 00128, Rome, Italy.

E-mail: riccardo.broglia@cnr.it

Department of Mechanical, Materials and Manufacturing Engineering, University Park, University of Nottingham, Nottingham, NG7 2RD.

E-mail: kwing-so.choi@nottingham.ac.uk

School of Mathematical Sciences, University of Nottingham, University Park, Nottingham, NG7 2RD, UK.

E-mail: paul.houston@nottingham.ac.uk

Aerospace Technology Centre, University of Nottingham, Innovation Park, Triumph Road, Nottingham, NG7 2TU, UK.

E-mail: laura.pasquale@nottingham.ac.uk

Department of Electrical and Electronic Engineering, University of Nottingham, University Park, Nottingham, NG7 2RD, UK.

E-mail: pericle.zanchetta@nottingham.ac.uk